Arabian Journal of Geosciences (2018) 11: 572
https://doi.org/10.1007/s12517-018-3877-8

ORIGINAL PAPER

High Nb–Ta rhyolites of the Kyihe region, north Daxingan Mountains, China: geochemistry, petrogenesis, and zircon U–Pb geochronology

Sun Guosheng[1] · Wang Qinghai[1] · Sun Jiuda[1] · He Xin[1] · Jin Ruixiang[1]

Received: 12 April 2018 / Accepted: 28 August 2018 / Published online: 27 September 2018

Abstract

Rhyolites with high Nb–Ta contents were recently discovered in the north Daxingan Mountains, China. We determined the geochemical characteristics and zircon U–Pb ages of these rhyolites to elucidate their tectonic setting of formation and petrogenesis. Zircons from the high Nb–Ta rhyolites are idiomorphic or hypidiomorphic, short prismatic crystals with oscillatory zoning; the zircon trace element has a higher Th/U ratio (> 0.4); zircon rare earth element (REE) content is high (average is 1729×10^{-6}) and indicates heavy REE (HREE) enrichment (average is 1561×10^{-6}) and shows positive Ce (Ce/Ce* = 2.1–103.4) and negative Eu (Eu/Eu* = 0.18–0.64) anomalies typical of crustal magmatic zircons. Their weighted-mean LA–ICP–MS U–Pb age of 155 ± 1 Ma indicates that they formed in the Upper Jurassic. The rhyolites are characterized by high SiO_2 and alkali contents and low Fe, Ca, Mg, and Mn contents, and are weakly peraluminous, indicating that they are high-K calc-alkaline rocks. Trace element compositions are characterized by enrichments in Nb, Ta, Zr, Hf, Ce, and Rb and depletions in Sr, Eu, Ba, P, Ti, Co, and Ni, with significant positive Ce (Ce/Ce* = 2.4–2.7) and negative Eu (Eu/Eu* = 0.06) anomalies. Niobium and Ta are hosted in the zircons. In $(Na_2O+K_2O+FeO^T+MgO+TiO_2)$ vs $(Na_2O+K_2O)/(FeO^T+MgO+TiO_2)$ and $(Al_2O_3+FeO^T+MgO+TiO_2)$ vs $Al_2O_3/(FeO^T+MgO+TiO_2)$ mineral characterization diagrams, data for the samples plot in the metamorphic greywacke or basic argillaceous rock fields, indicating that the magma originated from partial melting of crustal material. εSr(t) values cover a wide range (− 18.2 to + 102.9), whereas εNd(t) values have a narrow range (1.9–2.0) with T_{2DM} model ages of 789–785 Ma, indicating that the source was the Neoproterozoic Xinghua Ferry Group crustal basement. This crustal rock suite comprises a volcanic–sedimentary formation of metamorphosed mafic volcanic and terrigenous clastic rocks derived from a mixture of mantle and crustal materials. Residual phases in the source region include Ca-rich plagioclase, amphibole, orthopyroxene, and zircon + garnet. Together with the positive Ce anomalies and low-Sr/high-Yb characteristics of the rhyolites, this indicates that the source rocks melted at relatively shallow depths (< 30 km), low pressures (< 0.8 GPa), and high O_2 fugacity. Ga × 104/Al > 2.6, Ta vs Yb, and (Rb/30) vs Hf vs (3Ta) discrimination diagrams, data for the samples plot in the A-type rhyolite and intraplate granite fields, whereas in the Nb vs Y vs Ce diagram, the data plot in the A1-type field. It is concluded that an extensional tectonic setting, resulting from closure of the Mongolia–Okhotsk Ocean at the end-Triassic, or northward subduction of oceanic lithosphere under the Siberian Plate, caused underplating of mantle-derived basaltic magma and partial melting of metamorphic crustal rocks.

Keywords Daxingan Mountains · Volcanic rock belt · High Nb–Ta rhyolite · Zircon U–Pb chronology · Geochemistry · Petrogenesis

Introduction

The Daxingan Mountains' volcanic rock belt (DMVRB) is in the northern Xing–Meng orogenic belt in the eastern section of the Central Asian Orogenic Belt, China. It is distributed in NE-trending belts, stretching from the Chifeng Linxi–Udan area in the Inner Mongolia Autonomous Region in the south, to the Mohe County area of Heilongjiang Province in the north, with a length of ~ 1200 km and width of up to ~ 400 km. The DMVRB is widely covered by Mesozoic mafic and silicic volcanic rocks, with pre-Mesozoic strata being intermittently exposed. There are many polymetallic deposits in the area, including large and super-large deposits of nonferrous and precious metals, as well as rare earth element

✉ Sun Jiuda
1031748476@qq.com

[1] College of Earth Sciences, Jilin University, Changchun 130061, China

deposits (Shao et al. 1997, 1998; Shao and Zhang 1999; Ge et al. 2007a, b; Fan et al. 2003; Meng 2003;Wang et al. 2006; Zhang et al. 2008, 2010; Wu et al. 2011; Şengör et al. 1996; Li et al. 2006; Natal'in and Borukayev 1991; Zhou et al. 2009; Wu et al. 2007, 2011; Zhou et al. 2012; Liu et al. 2004). The geodynamic setting of the DMVRB remains unresolved, with suggestions including a mantle plume origin (Lin et al. 1998; Ge et al. 1999), a basin-and-range structural setting associated with closure of the Mongolia–Okhotsk Ocean and Paleo-Asian Ocean basin (Fan et al. 2003; Meng 2003), the influence of an extensional orogenic structure associated with Paleo-Pacific Plate subduction (Wang et al. 2006; Zhang et al. 2008, 2010, Zhao et al. 1994), and the influence of the Mongolia–Okhotsk and the circum-Pacific tectonic systems (Shao and Zhang 1999; Wu et al. 2011; Liu et al. 2004; Meng et al. 2011;Xu et al. 2009, 2011). The geodynamic setting of the DMVRB belt remains an important unresolved scientific issue.

Rhyolites with high Nb and Ta contents were recently discovered in the Kyihe region of the northern DMVRB, and these are the subject of our study. Such rhyolites have the potential to reveal the tectonic setting of Mesozoic volcanic rocks in the Daxingan Mountains, and the magma sources and origins of large-scale mineralization. The high Nb–Ta rhyolites are widely distributed in the area and have Nb_2O_5 contents of > 0.03 wt%, which classifies them as an industrial grade Nb–Ta deposit. Research into their petrogenesis is therefore of significance in exploration for similar rhyolites elsewhere in the region.

Regional geological background and rhyolite characteristics

The study area is located in the northern section of the DMVRB, in the northern Xingan Block (Zhou et al. 2016) (Fig. 1), adjacent to the main ridge fault of the Daxingan Mountains. The tectonic evolution of the area is complex and involved formation of a micro-continent with metamorphic basement in the Precambrian, closure of the Paleo-Asian Ocean and amalgamation of several micro-continents during the Paleozoic (Şengör et al. 1993), and superposition and transformation due to Mongolia–Okhotsk Ocean closure and Paleo-Pacific Plate subduction during the middle Cenozoic. The pre-Mesozoic structure has been removed by the Mesozoic tectonism and magmatism. Since the Mesozoic, the regional geological setting has been characterized by magmatic activity controlled by pre-Mesozoic basement faults, which created NE-, NNE-, and NNW-trending structures and magmatism.

The Precambrian rocks in the region form a lithostratigraphic unit composed of metaclastic and volcaniclastic rocks with minor carbonate intercalations, which are mainly distributed in the west and north of the DMVRB. The Xinghua Ferry Group is considered to represent Precambrian metamorphic basement of the Xingan Block (Ge et al. 2007a; Heilongjiang Bureau of Gology and Mineral Resources. Regional Geology of Heilongjiang Province 1993; Miao et al. 2007), including sillimanite–garnet-bearing gneiss, felsic gneiss, amphibolite, and graphite schist (Zhou et al. 2011a, 2016). Paleozoic strata are distributed mainly in the upper Heilongjiang depression in the north of the DMVRB, and exposed intermittently in the west and central–south of the belt. Jurassic–Cretaceous mafic and silicic volcanic and pyroclastic rocks are exposed widely in the study area, including the Tamulangou (J_2tm, J_2 and tm are abbreviations of the middle Jurassic and Tamulangou, respectively), Manketouebo (J_3mk, J_3 and mk are abbreviations of the upper Jurassic and Manketouebo, respectively), Manitu (J_3mn, mn is the abbreviation of Manitu), Baiyingaolao (K_1b, K_1 and b are abbreviations of the lower Cretaceous and Baiyingaolao, respectively), and Meiletu (K_1ml, ml is the abbreviation of Meiletu) groups. The Tamulangou Group contains volcanic and normal sedimentary rocks, comprising mainly gray–green, amygdaloidal, dense, massive basalt and its breccia, and trachyandesite with black silty mud. The Manketouebo Group comprises mainly silicic volcanic, pyroclastic, and sedimentary rocks. The Manitu Group comprises mainly dacite–dacitic and andesite–andesitic lithic tuff. The upper section of the Baiyingaolao Group comprises silicic volcanics, tuffs, and dacitic tuffs, whereas the lower section contains tuffaceous conglomerate, fine sandstone with silty shale, and small amounts of silicic tuff and volcanic rocks (animal and plant fossils are also found in this group). The Baiyingaolao Group unconformably overlies the intermediate volcanic rocks of the Manitu Group, and is unconformably covered by the Lower Cretaceous mafic–intermediate volcanic rocks of the Meiletu Group. The Meiletu Group comprises mainly a set of fumarolic, amygdaloidal, dense, massive trachyandesite, basalt, and its volcanic eruptions were dominated by lava and some debris flows. The Meiletu Group is distributed mostly as "islands" of higher ground and has a Lower Cretaceous age. In addition to the large-scale Mesozoic volcanic rocks, there are also extensive outcrops of granodiorite, granite porphyry, and other intermediate–silicic intrusive rocks.

The high Nb–Ta rhyolites are exposed in southern Kyihe County in the Oroqen Autonomous Banner, to the east of Wulukanggou. The widely exposed strata in the area represent the lower part of the Upper Jurassic Manketouebo Group (Fig. 1), which is distributed in a N–S direction over an area of ~ 2 km^2. The fresh rocks are gray with a porphyritic, felsitic, and weakly rhyolitic structure (Fig. 2a). Their phenocryst content is ~ 10%, and the phenocrysts comprise sanidine, quartz, and a small amount of black mica (Fig. 2b). The sanidine (~ 7%) is a high-temperature type with simply twinned crystals (2V = 63°, the term "2V" denotes the optical axial angle of a biaxial

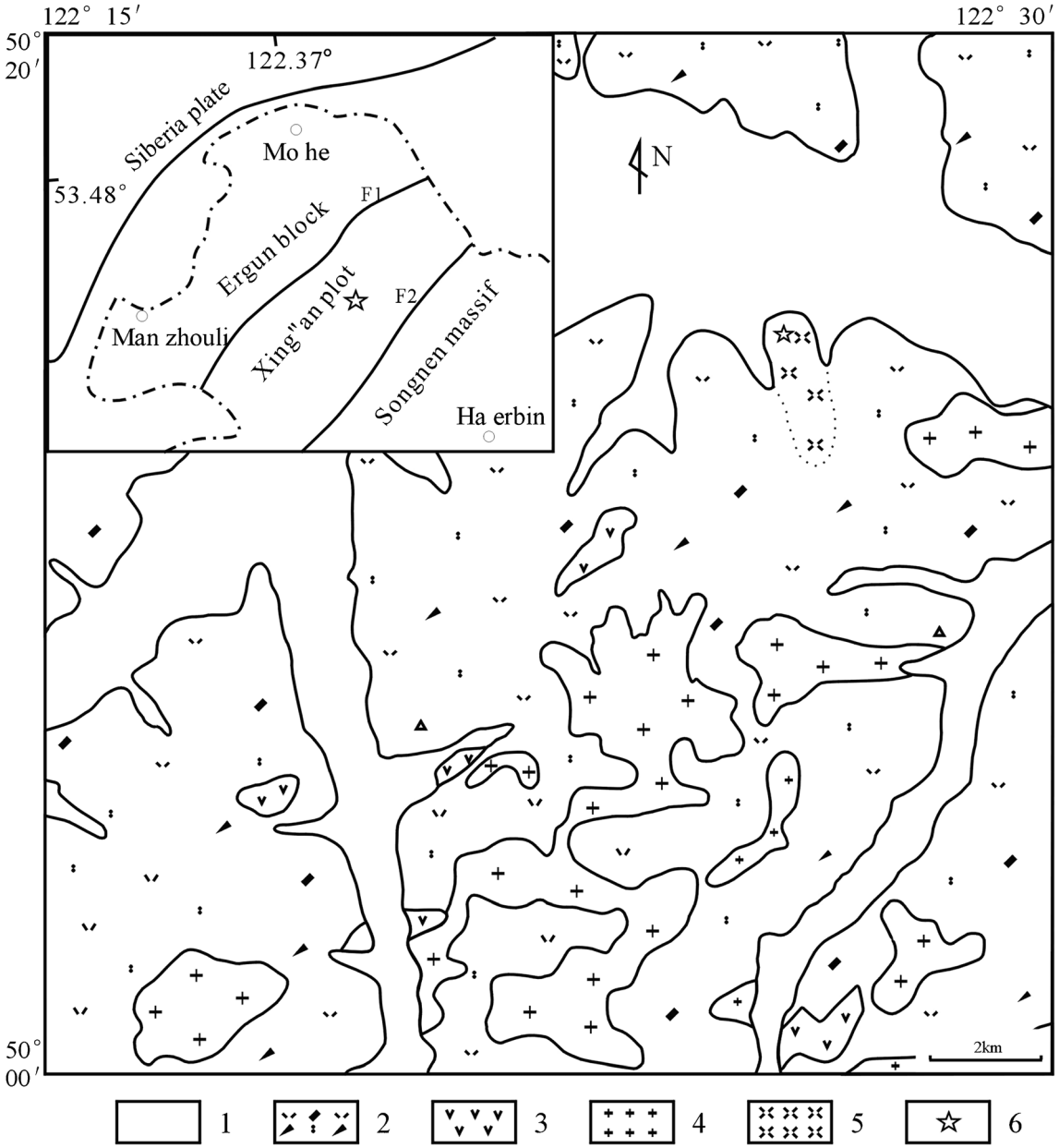

Fig. 1 Simplified geological map and sampling locations. (1) Quaternary; (2) the Upper Jurassic Manketouebo Group; (3) the Middle Jurassic Tamulangou Group; (4) Cretaceous granite porphyry; (5) rhyolite; and (6) sampling location. F1—the Tayuan-Xiguitu Fault; F2—the Heganshan-Heihe Fault

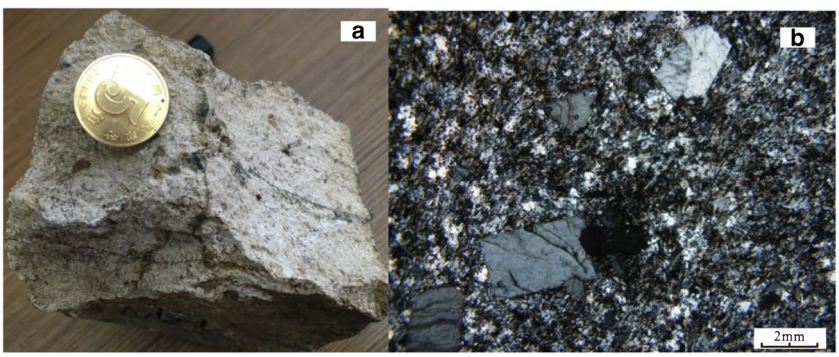

Fig. 2 Field photographs **a** and photomicrographs **b** of the samples

Table 1 Zircon U–Pb analytical data for rich Nb–Ta rhyolite

Spot	Pb	Th	U	Th/U	$^{207}Pb/^{206}Pb$		$^{207}Pb/^{235}U$		$^{206}Pb/^{238}U$		$^{207}Pb/^{206}Pb$		$^{207}Pb/^{235}U$		$^{206}Pb/^{238}U$	
	($\times10^{-6}$)				Isotopic ratio	1σ	Isotopic ratio	1σ	Isotopic ratio	1σ	Age (Ma)	1σ	Age (Ma)	1σ	Age (Ma)	1σ
IV-1	14	799	512	1.56	0.04928	0.00322	0.16744	0.01115	0.02464	0.00067	161	102	157	10	157	4
IV-2	16	923	591	1.56	0.04892	0.00789	0.16114	0.02576	0.02389	0.00089	144	264	152	23	152	6
IV-3	23	1594	759	2.10	0.04919	0.00294	0.16798	0.01022	0.02476	0.00069	157	89	158	9	158	4
IV-4	8	344	307	1.12	0.04846	0.00755	0.16361	0.02539	0.02448	0.00082	122	258	154	22	156	5
IV-5	11	515	403	1.28	0.04879	0.00584	0.16388	0.01969	0.02435	0.00069	138	213	154	17	155	4
IV-6	8	315	300	1.05	0.04903	0.00749	0.16667	0.0253	0.02465	0.00086	149	257	157	22	157	5
IV-7	21	1531	769	1.99	0.04922	0.00415	0.16722	0.01408	0.02463	0.00075	158	133	157	12	157	5
IV-8	22	1563	753	2.08	0.04889	0.00282	0.16457	0.00977	0.0244	0.00065	143	87	155	9	155	4
IV-9	13	638	488	1.31	0.04896	0.00518	0.16477	0.01745	0.0244	0.00074	146	180	155	15	155	5
IV-10	8	381	301	1.26	0.04882	0.00571	0.16514	0.01915	0.02453	0.00085	139	195	155	17	156	5
IV-11	12	689	448	1.54	0.04913	0.0019	0.16672	0.00688	0.0246	0.00065	154	50	157	6	157	4
IV-12	24	1667	812	2.05	0.04935	0.00432	0.16711	0.01455	0.02455	0.00078	164	137	157	13	156	5
IV-13	13	699	504	1.39	0.04907	0.00404	0.16431	0.01353	0.02428	0.00073	151	130	154	12	155	5
IV-14	20	1263	717	1.76	0.04961	0.00397	0.16658	0.01335	0.02435	0.00073	177	126	156	12	155	5
IV-15	11	522	414	1.26	0.04906	0.00352	0.16533	0.01201	0.02444	0.00070	151	111	155	10	156	4
IV-16	10	426	377	1.13	0.0489	0.00453	0.1648	0.01533	0.02444	0.00072	143	153	155	13	156	5
IV-17	11	551	440	1.25	0.04922	0.00257	0.16632	0.00893	0.02451	0.00068	158	74	156	8	156	4
IV-18	11	555	444	1.25	0.04916	0.00301	0.16514	0.01024	0.02436	0.0007	155	90	155	9	155	4
IV-19	11	568	417	1.36	0.04920	0.00492	0.16591	0.01643	0.02446	0.00082	157	160	156	14	156	5
IV-20	24	1653	791	2.09	0.04908	0.00388	0.16514	0.01308	0.0244	0.00073	152	123	155	11	155	5
IV-21	7	316	272	1.16	0.04917	0.00394	0.16616	0.01339	0.02451	0.00072	156	127	156	12	156	5

crystal), which have a euhedral–subhedral platy form, are 1–2 mm in diameter with micro-cracks, and mostly exhibit a porphyritic or glomeroporphyritic texture (Fig. 2c). The quartz (~ 3%) is euhedral–subhedral, granular or irregular in shape, 1–3 mm in diameter, and is visibly resorbed. Black mica is observed occasionally (< 1%) and is flaky and brown or reddish brown. The rhyolite matrix exhibits a felsitic and microcrystic texture, which is composed of small particles of xenomorphic, granular, or cryptocrystalline quartz and feldspar. Alkali feldspar microcrysts and xenomorphic granular quartz define the rhyolitic structure.

Analytical techniques

Major and trace element of rhyolites analyses were conducted at Jilin University, China. For major element analysis, six fresh rock samples were crushed to < 200 mesh in an agate mortar, fused into a glass disk at room temperature and pressure, and analyzed by X-ray fluorescence using an XRF-1500 spectrometer with an accuracy better than ± 1%. For trace element analyses (including rare earth elements; REE), 40-mg samples were dissolved in HF–HNO_3, diluted with 1% HNO_3, and analyzed using a dual-focus inductively coupled plasma mass spectrometer (ICP–MS) (Finnigan-MAT Element) with an accuracy better than ± 5%.

Zircon crystals were extracted by conventional gravitational and magnetic separation techniques and handpicked under a binocular microscope. The zircons were set in epoxy resin disks, which were then polished to about half thickness. Zircons with good crystal form were chosen for cathodoluminescence (CL) imaging, which were conducted at the Tianjin Institute of Geology and Mineral Resources, using a Gatan Mono CL3+CL system. Laser ablation inductively coupled plasma mass spectrometry (LA–ICP–MS) U–Pb dating was performed at the Laser Plasma Mass Spectrometry Laboratory, China University of Geosciences, using an Agilent 7500a spectrometer with a 193-nm laser system (New Wave UP 193SS). The ablation frequency was 10 Hz, beam diameter 30 μm, pre-ablation time 5 s, and ablation time 45 s. High-purity He was used as a carrier gas. Isotopic ratios were normalized on the basis of zircon standard 91500. Quality control samples included zircon standards TEMORA and Qinghu, and glass standards NIST612 and NIST614. Age calculations used the Isoplot program, and zircon U–Pb isotope ratios were calculated using the Glitter program 5.5. The glass standard NIST610 was used as an external standard and Si was used as an internal standard. Uncertainties on single data points are given at the 1σ level and on weighted means at the 2σ level.

Strontium and Nd isotopic analyses were conducted at the Tianjin Institute of Geology and Mineral Resources. Samples were dissolved in HF–$HClO_4$ (> 12 h at ~ 100 °C) and then purified by solvent extraction using HDEHP. Strontium and Nd contents and isotopic ratios were determined by thermal ionization mass spectrometry (TIMS) using a Triton TIMS system. Procedural blanks were Rb = 5.6×10^{-10} g; Sr = 3.8×10^{-10} g; Sm = 3.0×10^{-11} g; and Nd = 5.4 × 10–11 g.

The Nd–Sr isotopic ratios of the BCR-1 Nd and NBS-607 Sr standards obtained were $^{143}Nd/^{144}Nd = 0.512739 \pm 0.000005$ (2σ) and $^{87}Sr/^{86}Sr = 1.200050 \pm 0.000005$ (2σ), respectively. Mass fractionation corrections were based on internal standardization to $^{88}Sr/^{86}Sr = 8.37521$ and $^{146}Nd/^{144}Nd = 0.7219$.

Results

Zircon U–Pb dating

Twenty-one zircons were selected from the rhyolites for LA–ICP–MS U–Pb dating (Table 1). The samples appear pinkish brown in color, and most are hypidiomorphic–euhedral short prismatic crystals, with some being sub-angular crystals. Crystal diameters are 0.1–0.2 mm, with aspect ratios of 1:1 to 2:1. The zircons display magmatic oscillatory zoning (Fig. 3). Zircon total REE content (∑REE) is 655–4926 × 10^{-6}, and the light REE to heavy REE ratio (LREE/HREE) is 0.03–0.19, indicating significant REE fractionation and HREE enrichment (Table 2). The REE partition diagram shows that the whole REE patterns decline to left (Fig. 4a). The zircons display positive Ce anomalies (Ce/Ce* = 2.1–103.4) and negative Eu anomalies (Eu/Eu* = 0.18–0.64), consistent with characteristics of crustal magmatic zircons (Hoskin and Schaltegger 2003). Cerium exists in magma as Ce^{3+} and Ce^{4+}, and the latter can easily replace Zr^{4+} and enter the zircon lattice during crystallization, thus fractionating Ce from other REEs. Under high oxygen fugacity (fO_2) conditions, the higher Ce^{4+}/Ce^{3+} ratio provides more Ce^{4+} for the zircon lattice, resulting in strongly positive Ce anomalies (Ballard et al. 2002; Zhao 2010a; Burnham and Berry 2012). The high Nb–Ta rhyolites are therefore considered to have formed in high-fO_2 conditions. Eu exists mainly as Eu^{3+} and cannot be fractionated from other trivalent REEs under high-fO_2 conditions. The negative Eu anomalies are thus inherited from low-Eu magma (Mass et al. 1992).

Zircon Th and U contents vary widely, with Th = 315–1669 × 10^{-6} (average 834 × 10^{-6}) and U = 272–812 × 10^{-6} (average 515 × 10^{-6}). Th/U ratios of 1.05–2.10 (average 1.50) indicate that the zircons formed by magmatic crystallization. The zircon $^{206}Pb/^{238}U$ ages vary from 158 to 152 Ma, with the concordia diagrams (Fig. 4b) indicating that the data are concordant and define a weighted-mean age of 155.9 ± 1.0 Ma (MSWD = 0.25; $n = 21$), which represents an Upper Jurassic age for the rhyolite.

Geochemical characteristics

Major elements

Major element compositions of the high Nb–Ta rhyolites are given in Table 3. Their SiO_2 contents (71.9–72.1 wt%) are high, consistent with their silicic nature. The rhyolites have a moderate Al_2O_3 content (13.8 wt%), with an average aluminum saturation index (A/CNK) of 1.06, indicating a weakly peraluminous rock type. The total alkali (K_2O+Na_2O) content is relatively high (average 9.2 wt%), with an average K_2O/Na_2O ratio of 0.93, indicating an Na-rich rhyolite. FeO^T (2.5–2.6 wt%), CaO (0.2 wt%), TiO_2 (0.1 wt%), and MgO (0.1 wt%) contents are low. In the total alkalis–silica (TAS) diagram (Fig. 5a), data for the rhyolite samples plot as subalkaline series rocks. Rittmann index ($\sigma = (Na_2O+K_2O)^2/(SiO_2–43)$; wt%) values of ~2.9 wt% indicate that the rocks

Fig. 3 Representative CL images of zircons from the high Nb–Ta rhyolites

Table 2 Rare earth element composition of zircons LA–ICP–MS

Sample No.	1	2	3	4	5	6	7	8	9	10	11	12	13	14	15	16	17	18	19	20	21
La	1.19	2.08	0.68	19.09	0.77	0.05	0.33	0.23	0.08	0.02	0.36	34.77	0.11	0.49	15.47	0.10	0.39	0.87	0.02	0.02	1.24
Ce	196.09	199.85	140.07	97.44	198.02	90.34	41.39	80.44	114.68	99.73	570.55	140.56	93.82	91.25	98.71	57.71	116.99	177.42	11.57	51.42	41.05
Pr	1.54	1.56	0.78	2.99	0.95	0.30	0.29	0.24	0.50	0.29	3.00	6.63	0.27	0.72	4.97	0.25	0.76	1.65	0.13	0.22	0.59
Nd	13.55	16.11	11.59	15.08	9.60	4.70	3.90	5.47	7.86	5.29	49.11	27.39	4.21	8.25	27.07	2.55	10.58	18.60	2.55	3.59	6.37
Sm	18.45	25.74	22.18	11.05	18.27	8.14	7.99	5.11	18.06	8.18	78.86	19.16	8.01	12.89	11.69	5.07	15.99	30.38	4.15	6.00	8.92
Eu	4.52	10.15	10.03	4.55	7.14	2.38	3.92	1.77	6.65	1.98	25.92	6.72	3.44	5.42	2.73	1.65	5.11	4.24	2.19	2.75	2.49
Gd	66.09	120.17	112.88	49.35	86.18	35.99	43.10	26.26	92.32	32.67	274.40	83.36	35.61	55.89	37.97	20.63	67.46	122.95	18.71	25.04	38.06
Tb	20.82	39.28	35.59	16.75	26.77	11.63	15.52	9.39	32.08	9.42	76.50	26.33	12.04	18.62	11.43	7.65	21.12	38.99	6.06	8.15	13.08
Dy	214.24	426.04	387.05	196.85	286.46	133.74	183.20	113.62	377.82	98.33	750.87	279.39	139.15	213.02	127.25	92.77	231.77	402.84	74.59	91.65	152.59
Ho	71.02	148.22	134.48	74.80	97.82	49.16	69.14	42.37	137.65	34.39	239.97	97.56	52.97	76.72	45.66	36.53	80.98	129.85	29.01	34.31	57.10
Er	283.87	606.00	547.30	329.09	393.57	212.46	304.39	194.74	578.64	138.67	916.16	414.03	232.59	332.13	192.36	177.76	330.57	498.34	134.02	148.95	254.51
Tm	53.88	117.46	105.77	68.26	73.86	43.64	63.35	42.65	113.91	27.46	172.72	82.01	48.01	67.68	38.79	39.72	63.30	90.16	28.41	31.16	51.98
Yb	467	1056	947	646	657	408	609	417	1048	258	1502	770	464	641	355	408	578	762	284	300	508
Lu	81	193	175	124	119	80	117	79	192	50	266	144	93	123	66	81	107	131	59	59	97
Y	2036	4384	3972	2233	2810	1418	2097	1319	4107	944	6727	2934	1551	2306	1322	1153	2319	3581	887	993	1683
ΣREE	1494	2961	2630	1655	1975	1081	1463	1018	2720	764	4926	2132	1187	1647	1035	931	1630	2409	655	763	1232
LREE	235	255	185	150	235	106	58	93	148	115	728	235	110	119	161	67	150	233	21	64	61
HREE	1258	2706	2445	1505	1740	975	1405	925	2572	649	4199	1897	1077	1528	875	864	1480	2176	634	699	1172
LREE/HREE	0.19	0.09	0.08	0.10	0.13	0.11	0.04	0.10	0.06	0.18	0.17	0.12	0.10	0.08	0.18	0.08	0.10	0.11	0.03	0.09	0.05
Eu/Eu*	0.35	0.46	0.50	0.50	0.46	0.36	0.52	0.38	0.40	0.32	0.48	0.44	0.53	0.52	0.36	0.43	0.41	0.18	0.64	0.59	0.35
Ce/Ce*	30.15	25.97	41.31	2.84	48.91	88.02	30.57	76.19	67.12	103.36	56.33	2.12	94.54	30.83	2.74	62.45	39.85	27.51	26.17	69.40	11.74

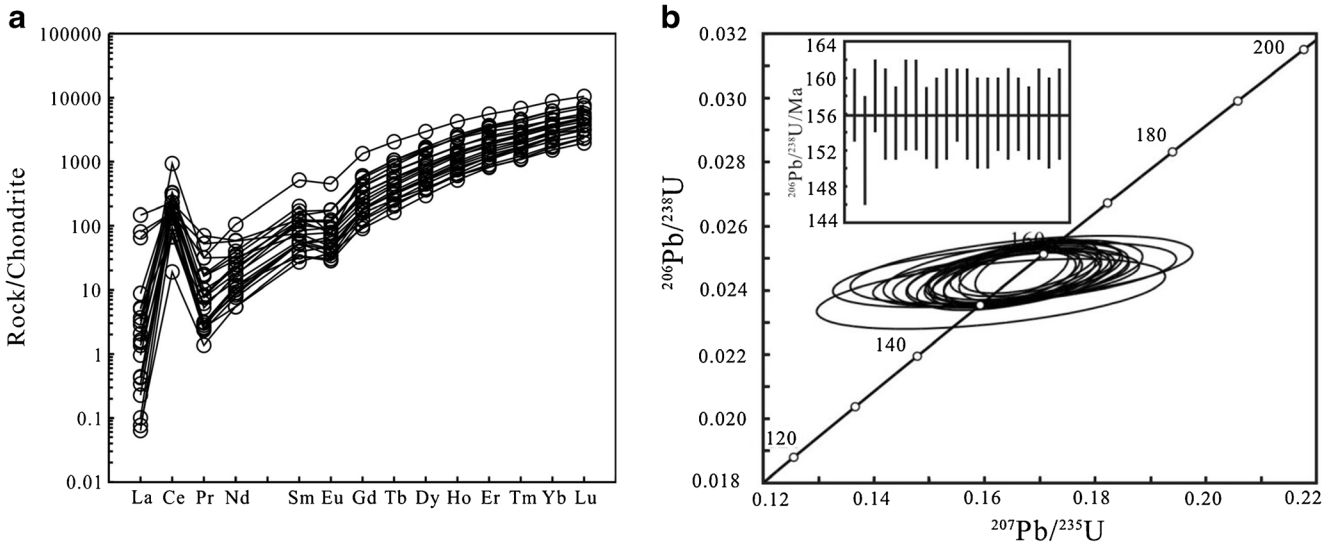

Fig. 4 Zircon chondrite-normalized REE distribution patterns **a** and LA–ICP–MS zircon U–Pb concordia diagrams **b** of rich high Nb–Ta rhyolite

are of the calc-alkaline series, and in the K_2O vs SiO_2 diagram (Fig. 5b), the samples plot in the high-K calc-alkaline field. In summary, the high Nb–Ta rhyolites of the Kyihe region are high-Si, low-Ti, peraluminous, high-K calc-alkaline series rocks.

Trace elements

The rhyolite REE content is high with ΣREE = 326–344 × 10^{-6} (Table 3; Fig. 6a), ΣLREE = 284–305 × 10^{-6}, ΣHREE = 38.3–39.6 × 10^{-6}, and LREE/HREE = 7.4–8.0. $(La/Yb)_N$ ratios (3.8–4.5) indicate that there was significant fractionation between LREE and HREE, with LREE enrichment, while (La/Sm)N ratios of 4.8–5.5 also indicate significant LREE fractionation. The ΣHREE content is about ten times that of standard chondrite. $(Gd/Yb)_N$ ratios (1.26–1.34) and relatively flat HREE patterns (Fig. 6a), with no obvious fractionation, indicate that a significant amount of garnet was incorporated in the source magma. The greater Yb_N content (28.9 × 10^{-6}) than Ho_N (24.1 × 10^{-6}) indicates a slight loss of middle REEs, suggesting residual amphibole was present in the magma source. The rhyolites exhibit an obvious positive Ce anomaly (Ce/Ce* = 2.44–2.67), indicating that the rocks were formed in a strongly oxidizing environment with melting and enrichment of Ce-bearing minerals. The negative Eu anomalies (Eu/Eu* ~ 0.06) are due to residual Ca-rich plagioclase in the source, which could also explain the low Ca, Sr, and Ba contents (alteration such as sericitization or albitization was not observed in the rhyolite, and so reactions between volatile fluids containing F and Cl were not involved). Enrichment in Nb, Ta, Zr, Hf, Rb, Th, and Ce and depletion in Sr, Ba, P, and Ti are evident in the trace elements data (Table 3) and spider diagrams (Fig. 6b). High Th/U (4.94–5.12) and Rb/Sr (12.0–13.5) ratios indicate that the source rocks were associated with continental crustal materials and/or residual minerals such as plagioclase, rutile, and apatite during melting. Rhyolite Zr contents are in the range of 804–892 × 10^{-6}, whereas compatible elements such as Co (1.4–2.0 × 10^{-6}), Ni (1.6–2.0 × 10^{-6}), and V (2.1–2.3 × 10^{-6}) have low contents, indicating that Zr-rich minerals were incorporated during melting, whereas Fe- and Mg-rich minerals such as pyroxene remained as residue minerals in the source. Sr and Yb contents of 18.5–20.6 × 10^{-6} and 7.0–7.3 × 10^{-6}, respectively, indicate that the rock is a low-Sr/high-Yb (Zhang et al. 2006) rhyolite.

Sr and Nd isotopic compositions

Properties of magma sources can sometimes be inferred from Sr and Nd isotopic compositions, and these results are given in Table 4. Rhyolite Rb/Sr ratios are relatively high (12.0–13.5), whereas Sm/Nd ratios are low (0.28). ($^{87}Sr/^{86}Sr$)i ratios and εSr(t) values are in the ranges of 0.70300–0.71160 and − 18.21 to 102.94. The variability of these data is indicated by four of the five samples having positive εSr(t) values and one a negative value, whereas three samples have ($^{87}Sr/^{86}Sr$)i ratios in the range 0.7040–0.7060 and two have ratios of > 0.7060. ($^{143}Nd/^{144}Nd$)i ratios and εNd(t) values are in the ranges of 0.512537–0.512539 and 1.9–2.0, respectively, similar to those of granites in continental crust in the Xing–Meng orogenic belt (Mcdonough and Sun 1995; Hong et al. 2000, 2003), indicating that the magma was derived from weakly or undepleted mantle (Shao et al. 1998; Shao and Zhang 1999). The relative deviation of the Sm/Nd ratio from the chondritic value, *f*Sm/Nd (*f*Sm/Nd = ($^{147}Sm/^{144}Nd$ –($^{147}Sm/^{144}Nd$)CHUR)/($^{147}Sm/^{144}Nd$)CHUR) is in the range of 0.09 and 0.5 for the rhyolites, and slightly different from the average crustal value (0.118) indicating differentiation of ^{147}Sm and ^{144}Nd during melting and metamorphism. This may distort model ages, although fractionation of Sm and Nd in the source is not obvious. As such, the two-stage Nd isotopic model age

Table 3 Contents of major elements (wt%) and trace elements ($\times 10^{-6}$) of high Nb–Ta of rhyolite

Spot	IV-1	IV-2	IV-3	IV-4	IV-5	IV-6	Average
SiO_2	72.08	72.1	71.89	72.02	72.12	72.05	72.04
Al_2O_3	13.78	13.78	13.79	13.8	13.8	13.82	13.8
Fe_2O_3	2.61	2.61	2.6	2.51	2.63	2.45	2.57
FeO	0.19	0.19	0.17	0.23	0.19	0.28	0.21
CaO	0.22	0.23	0.22	0.22	0.22	0.22	0.22
MgO	0.09	0.08	0.09	0.08	0.09	0.08	0.09
K_2O	4.43	4.42	4.42	4.42	4.4	4.41	4.42
Na_2O	4.75	4.74	4.76	4.77	4.76	4.74	4.75
TiO_2	0.12	0.13	0.13	0.13	0.12	0.13	0.13
MnO	0.15	0.15	0.15	0.15	0.15	0.15	0.15
P_2O_5	0.02	0.02	0.02	0.02	0.02	0.02	0.02
K_2O+Na_2O	9.18	9.16	9.18	9.19	9.16	9.15	9.17
FeO^T	2.54	2.54	2.51	2.49	2.56	2.48	2.52
$FeO^T/(FeO^T+MgO)$	0.97	0.97	0.97	0.97	0.97	0.97	0.97
LOI	1.13	1.13	1.14	1.16	1.14	1.09	1.13
Total	99.58	99.58	99.38	99.51	99.65	99.44	99.53
La	44.17	38.66	38.14	39.74	38.38	37.84	39.49
Ce	212.94	210.2	207.04	206.16	204.83	201.61	207.13
Pr	9.44	9.01	8.77	9.12	8.72	8.71	8.96
Nd	30.52	28.92	27.95	29.28	27.99	27.97	28.77
Sm	8.09	8.09	7.88	7.97	7.92	7.90	7.98
Eu	0.16	0.16	0.16	0.18	0.16	0.15	0.16
Gd	9.39	9.38	9.19	9.28	9.17	9.14	9.26
Tb	1.70	1.74	1.70	1.70	1.70	1.70	1.71
Dy	9.76	10.2	9.98	9.90	9.98	9.83	9.94
Ho	2.03	2.12	2.09	2.05	2.06	2.06	2.07
Er	6.32	6.62	6.50	6.38	6.44	6.41	6.45
Tm	1.04	1.1	1.08	1.04	1.06	1.06	1.06
Yb	7.01	7.34	7.28	7.08	7.18	7.14	7.17
Lu	1.00	1.06	1.05	1.01	1.03	1.01	1.03
ΣREE	343.56	334.61	328.81	330.86	326.6	322.55	331.17
LREE/HREE	7.98	7.46	7.46	7.61	7.46	7.41	7.56
La_N/Yb_N	4.52	3.78	3.76	4.03	3.83	3.80	3.95
La_N/Sm_N	5.46	4.78	4.84	4.99	4.85	4.79	4.95
Eu/Eu*	0.06	0.06	0.06	0.06	0.06	0.06	0.06
Ce/Ce*	2.44	2.66	2.67	2.56	2.64	2.62	2.60
Li	10.73	10.89	10.8	11	10.86	10.96	10.87
Sc	1.08	1.16	1.07	1.24	1.08	1.03	1.11
Y	62.49	64.88	64.13	63.25	64.25	63.64	63.77
Be	8.51	8.61	8.53	8.53	8.61	8.52	8.55
V	2.14	2.18	2.23	2.29	2.16	2.11	2.19
Co	1.35	2.02	1.43	1.46	1.40	1.35	1.50
Ni	1.61	1.83	1.99	1.81	1.72	1.56	1.75
Ga	30.48	30.05	30.34	30.26	30.91	30.97	30.5
Rb	244.42	252.05	247.58	247.45	249.00	251.08	248.6
Sr	18.68	19.2	19.4	20.6	18.46	18.66	19.17
Ba	72.55	72.04	73.01	76.73	72.38	72.4	73.19
Nb	183.32	185.27	185.00	187.70	186.69	186.22	185.70
Ta	10.24	10.44	10.48	10.51	10.38	10.52	10.43
Zr	813.72	884.48	892.3	804.44	834.79	836.56	844.38
Hf	27.12	28.78	29.34	27.31	27.59	27.91	28.01
Th	27.39	28.04	27.54	27.92	27.54	27.53	27.66
Pb	52.04	33.36	32.84	33.69	32.99	33.22	36.36
U	5.35	5.56	5.57	5.45	5.46	5.46	5.48
Nb/Ta	17.9	17.75	17.65	17.86	17.99	17.70	17.81
Zr/Hf	30.00	30.73	30.41	29.46	30.46	29.97	30.15
Th/U	5.12	5.04	4.94	5.12	5.04	5.04	5.05
Rb/Sr	13.08	13.13	12.76	12.01	13.49	13.46	12.97

(T_{2DM}) may better represent the age of the source materials remaining in the crust. The T_{2DM} age of the rhyolites is 789–785 Ma, and older than granites in the Central Asian Orogenic Belt (700–600 Ma) (Hong et al. 2000, 2003; Guo et al. 2014). This relatively old formation age suggests that there was a crustal growth event during the Neoproterozoic, with crustal materials

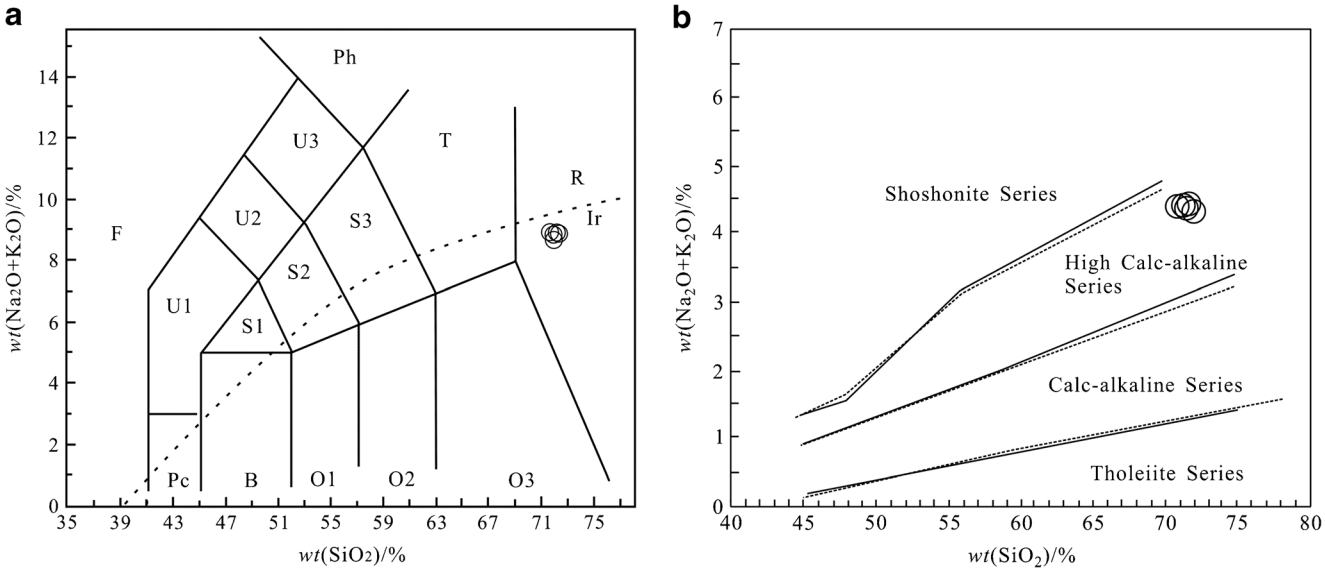

Fig. 5 Plots of SiO_2 vs (SiO_2+K_2O) (**a**) and plots of SiO_2 vs K_2O (**b**) for high Nb–Ta rhyolite

originating from depleted mantle or partial melting of juvenile crust. In a ($^{87}Sr/^{86}Sr$)i vs ($^{143}Nd/^{144}Nd$)i diagram (Fig. 7) (Zindler and Hart 1986), data for the samples plot in the upper region of the fourth quadrant, with three plotting in the depleted mantle field and two in the enriched mantle field, indicating that partial melting of juvenile crust may have been the main source of the high Nb–Ta rhyolitic magma.

Age and tectonic setting

Rhyolite age

Mesozoic volcanic rocks of the Daxingan Mountains include, from older to younger, the Tamulangou, Manketouebo, Manitu, Baiyingaolao, and Meiletu groups. The high Nb–Ta rhyolite of the Kyihe area is located in strata within the Manketouebo Group which, in turn, is located within the lower–middle layers of the DMVRB. The Manketouebo Group comprises volcanic strata containing silicic volcanic, pyroclastic, and epiclastic rocks. These volcanic rocks have been considered as being the first section of the Lower Cretaceous Guanghua Group (Qu 1997), although collectively they are considered to be within the Manketouebo Group (Wu 1996). Recent zircon LA–ICP–MS U–Pb dating indicates that the Manketouebo Group can be divided into two age groups of 143–132 Ma (Zhang et al. 2014; Ji 2017; Du et al. 2017; Zhou and Jiang 2017; Wang et al. 2017) and 160–151 Ma (Yang et al. 2012; Zhang 2009; Chen et al. 2012; Li et al. 2016), with the former belonging to the Baiyingaolao Group and the latter being the eruptive ages of the volcanic rocks of the Manketouebo Group. The mean zircon U–Pb age of the

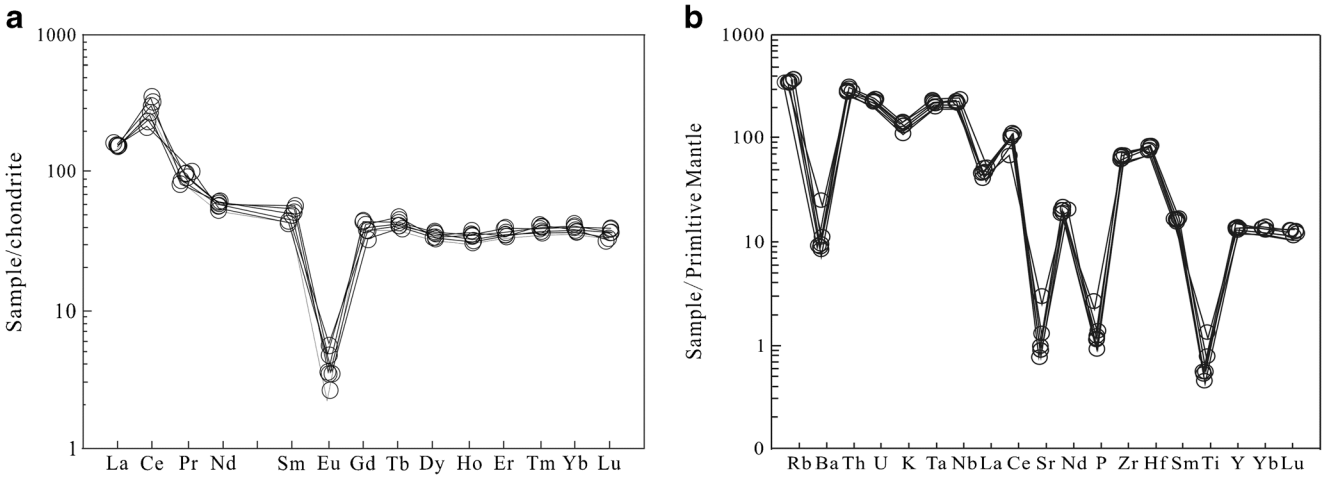

Fig. 6 Chondrite-normalized REE patterns (**a**) and primitive mantle-normalized spidergram (**b**) of high Nb–Ta rhyolite (normalization values after Sun and Mc Donogh, 1989). Mesozoic post-orogenic igneous rocks in Northeast China (from Wu et al., 1997). Mesozoic igneous rocks in northeastern Inner Mongolia (from Zhou et al., 2003)

Table 4 Sr–Nd isotopic results of high Nb–Ta rhyolite

	$^{87}Rb/^{86}Sr$	$^{87}Sr/^{86}Sr$	$^{147}Sm/^{144}Nd$	$^{143}Nd/^{144}Nd$	t/Ma	εSr(0)	εSr(t)	$f_{Rb/Sr}$	$(^{87}Sr/^{86}Sr)_i$	εNd(0)	εNd(t)	$f_{Sm/Nd}$	T_{DM}	T_{2DM}	$(^{143}Nd/^{144}Nd)_i$
IV-1	38.131	0.781353	0.1676	0.512709	155	1090.89	14.33	157.22	0.70533	1.4	2.0	−0.15	1463	785	0.512539
IV2	38.256	0.781105	0.1769	0.512716	155	1087.37	7.29	157.74	0.70483	1.5	1.9	−0.10	1802	789	0.512537
IV-3	37.192	0.781726	0.1783	0.51272	155	1096.18	46.29	153.32	0.7076	1.6	2.0	−0.09	1855	785	0.512539
IV-4	35.006	0.781295	0.1721	0.512712	155	1090.06	102.94	144.25	0.7116	1.4	1.9	−0.12	1610	788	0.512537
IV-5	39.308	0.781333	0.1789	0.512718	155	1090.60	−18.21	162.10	0.7030	1.6	1.9	−0.09	1898	789	0.512537

Kyihe rhyolites has been determined in the present study to be 156 ± 1 Ma (MSWD = 0.25; $n = 21$), consistent with the volcanic rocks of the Manketouebo Group (160–151 Ma). Field characteristics of the rhyolites also match those of the Manketouebo Group, which is conformably overlain by andesite of the Manitu Group in the north of the study area. The high Nb–Ta rhyolite is thus considered to be the product of the Manketouebo volcanic eruption cycle during the Upper Jurassic.

Tectonic setting

Previous studies have indicated that the Songliao Basin and the area to the east of it were influenced by the Mesozoic Pacific rim tectonic system, whereas areas to the west of the basin and on the northern margin of the North China Block (including the Xingan Block) (Zhao et al. 1994; Xu et al. 2013) were influenced by the Mongolia–Okhotsk Ocean tectonic system. However, the subduction direction and closure time of the Mongolia–Okhotsk Ocean are unresolved. Some studies indicate that the ocean was closed in the Triassic (Maruyama et al. 1997), whereas others suggest that this took place in the Upper Jurassic–Lower Cretaceous (Cogné et al. 2010; Metelkin et al. 2010; Pei et al. 2011). Some studies have suggested that the Mongolia–Okhotsk oceanic lithosphere was subducted northward under the Siberian Plate during the late Permian (Meng 2003; Voo et al. 1999; Zorin 1999), whereas others have suggested that the formation of Triassic porphyry Cu–Mo deposits and granites in the Ergun Block was related to southward subduction (Wu et al. 2011; Jiang et al. 2010; Chen et al. 2010; Zeng et al. 2014).

Permian–Lower Jurassic sedimentary strata are not evident in the DMVRB, which would have been subjected to uplift and erosion, although in the Middle Jurassic, a series of faults and depressions developed from north to south in the Daxingan Mountains, including the Mohe basins, middle Daxingan Mountains' fault zone, and Longjiang, Hailar, and Tuquan basins (HBGMRRGHP 1993; Zhao et al. 2014). The Emuerhe Group, in the upper Heilongjiang depression, formed in the Middle–Upper Jurassic, whereas sediments of the Xiufeng Group were deposited as late as the Middle Jurassic (Zhao et al. 2014). Both normal and listric faults developed during extensional activity in the south part of the Mohe basins, which has the characteristics of a fault basin, indicating that the formation age was earlier than the Middle Jurassic (Shi et al. 2014). The Wanbao Group, which comprises coarse-grained sediments of terrestrial fluvial facies, developed between the Daxingan Mountains' fault, Longjiang fault basin, and Tuquan basin and has a zircon age for

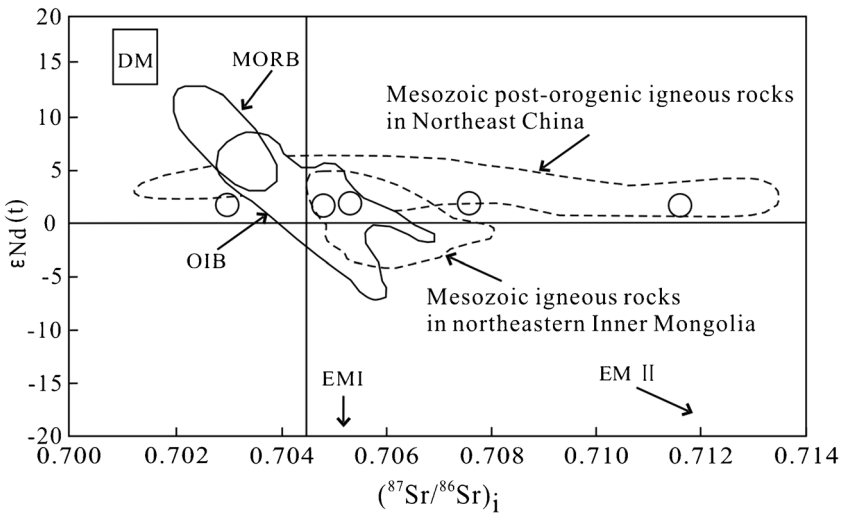

Fig. 7 Diagram of εNd(t) vs $(^{87}Sr/^{86}Sr)$ for source discrimination

intercalated volcanic rocks of 165.2 ± 1.7 Ma (Zhang et al. 2017), indicating that they formed at the end of the Middle Jurassic (HBGMRRGHP 1993; Inner Mongolia Bureau of Geology and Mineral Resources. Regional geology of Inner Mongolia 1991; Bao et al. 2011; Wang et al. 2013a). Furthermore, the rifting period of the Hailar fault basin coincided with the eruption of the Middle Jurassic Tamulangou Group (Zhao 2010b). It can therefore be concluded that the Daxingan Mountains' crust had been thickening until the end of the Lower Jurassic, with the region having been in an extensional tectonic setting since the beginning of the Middle Jurassic. The Mesozoic occurrence of volcanic activity in the Daxingan Mountains indicates that crustal evolution involved mantle-derived magma in an extensional tectonic setting within the continental lithosphere, but was not associated with magmatic activity in the subduction system of the active continental margin (Shao and Zhang 1999).

Tectonic settings are distinguished in the (Rb/30) vs Hf vs (3Ta) and Rb vs (Y+Nb) diagrams (Fig. 8a, b), where data for the Kyihe rhyolite samples plot in the intraplate granite field. A1/A2 tectonic settings are distinguished in the Nb vs Y vs Ce diagram (Fig. 8c), where data for the samples plot in the A1 field, indicating that the rocks were formed in an intraplate extensional tectonic setting associated with rifting, mantle plumes, and hot spots, rather than in an extensional setting developed by post-collisional or post-orogenic collapse of continental crust. Recent studies have indicated that volcanic rocks of the Upper Jurassic Manitu and Lower Cretaceous Baiyingaolao groups were also formed in an intraplate extensional tectonic setting (Sun et al. 2011; Gou et al. 2010). The study area had thus been in an intraplate extensional tectonic setting during the Upper Jurassic–Lower Cretaceous, with the Mongolia–Okhotsk Ocean having been closed, or oceanic lithosphere subducted northward under the Siberian Plate, during the Upper Triassic–Lower Jurassic. The resulting extension of the Xingan Block in the southern Mongolia–Okhotsk Ocean caused emplacement of the A-type granites (widely exposed in the study area) and large-scale eruption of high-K calc-alkaline magmas.

Petrogenesis and magma sources

Petrogenesis

Major element compositions of the Kyihe high Nb–Ta rhyolites are characterized by high SiO_2 and K contents and low Ca and Mg contents, while trace element compositions are characterized by enrichment in Nb, Ta, Zr, Hf, Rb, Th, U, and Ce and depletion in Sr, Ba, Ti, and P. Their REE patterns exhibit a "V" shape with obvious negative Eu anomalies. $Ga \times 10^4/Al > 2.6$, the rhyolite thus has a composition similar to A-type granite (Zhang et al. 2012; Whalen et al. 1987). A-type granites are formed under alkali-rich, anhydrous, and anorogenic conditions by the melting of source rocks under low-pressure and high-temperature conditions (Loiselle and Wones 1979; Zhang et al. 2007). A hydrous and high viscosity A-type granitic magma has a similar density to that of rock-forming minerals and does not undergo crystallization differentiation. The lack of cumulates associated with the rhyolite, and synchronous intermediate–mafic igneous rocks in the study area, further indicates that there was no crystallization differentiation of granitic magma (Zhang et al. 2007, 2012; Reid et al. 1993), with the chemical composition also indicating that there was no mixing of mafic and silicic magmas. Magmatic processes are distinguished by the La/Sm vs La diagram (Fig. 9), where data for the samples plot on an oblique line as a result of partial melting. It is concluded that the geochemical and Sr–Nd isotopic compositions indicate that the rhyolitic magma originated from partial melting of crustal materials.

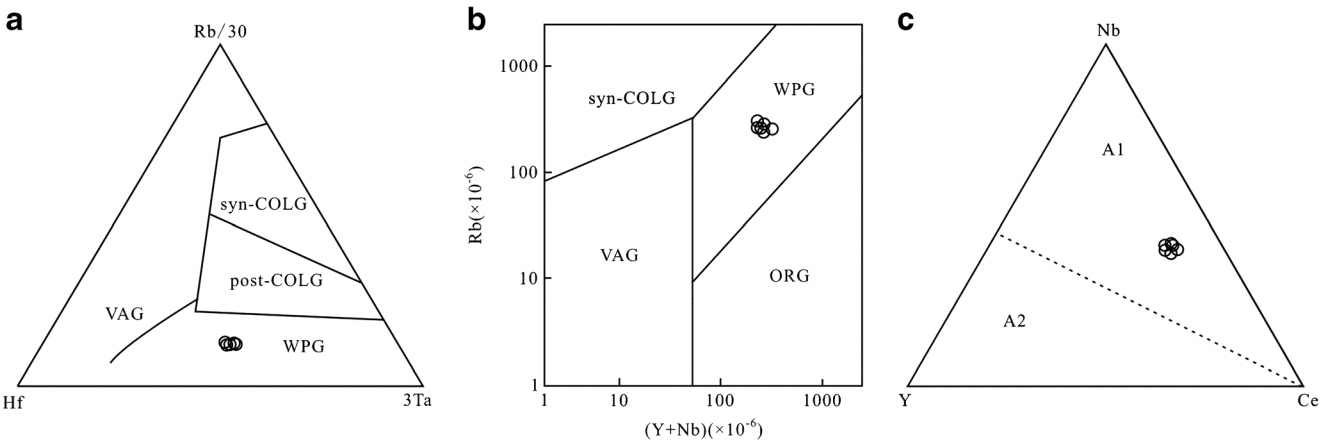

Fig. 8 Diagrams for discriminating tectonic setting of Hf-Rb/30-Ta × 3 (**a**), Y+Nb-Rb (**b**), and Y-Nb-Ce (**c**) for high Nb–Ta rhyolite

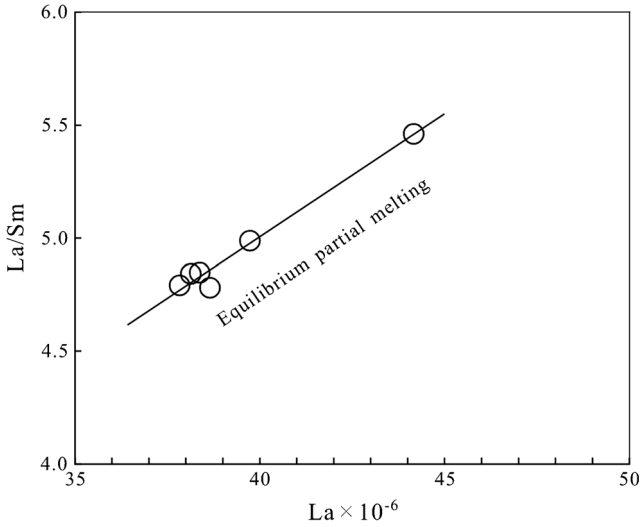

Fig. 9 Discrimination diagram of La-La/Sm for high Nb–Ta rhyolite

Magma source

Major and trace element compositions, Ce and Eu anomalies, and Sr–Nd isotopic compositions provide indications of the nature of the rhyolite magma source, as discussed in the following sections.

Nb, Ta, and Zr

The most distinctive trace element characteristics of the rocks are their high Nb (183–188 × 10^{-6}), Ta (10–11 × 10^{-6}), and Zr (804–892 × 10^{-6}) contents, which provide important clues concerning properties of the magma source.

Nb, Ta, and Zr contents increase as the volcanic lithology changes from mafic to silicic and tholeiitic to alkaline (Liu 1987). Ocean island basalt (OIB) formed from alkaline basaltic magma has the highest Nb (48 × 10^{-6}) and Ta (2.7 × 10^{-6}) contents (Zhao et al. 2008; Sun et al. 1989) of mantle materials, with Nb and Ta being hosted primarily in Ca- and Ti-rich minerals such as rutile, titanite, perovskite, Fe–Ti oxides, and allanite, and secondarily in Fe- and Mg-rich minerals such as pyroxene, hornblende, and biotite (Liu 1987). The low Ca, Ti, Fe, and Mg contents of the rhyolite thus indicate that its source is independent of such minerals, with no genetic connection to alkaline basaltic rocks.

The Zr contents of the Kyihe rhyolites are in the range of 813–892 × 10^{-6}, whereas that of high Nb–Ta sodium amphibole rhyolite in the Aliwula region (in the southern segment of the Daxingan Mountains) is 8528–15,560 × 10^{-6} (Wang et al. 2013b) indicating large-scale Zr enrichment in the source area. The Zr ionic radius is similar to those of Nb and Ta, and so the latter can replace Zr in the crystal lattice, forming naegite rich in Nb, Ta, and REEs, with zircon becoming the main carrier of Nb and Ta. However, as an accessory mineral, the zircon content of primary magmatic rocks is very low. Its origin may therefore be more related to coastal or continental clastic rocks.

During weathering, placer sediments in riverbed and coastal environments tend to become enriched in Nb, Ta, and Zr, with ~24% of Nb, Ta, and Zr mining involving placer deposits (Liu 1987; Mou 1999). We speculate that coastal or continental clastic rocks rich in Nb, Ta, and Zr are present in the underlying continental crustal rocks, and these may have participated in the formation of the high Nb–Ta rhyolite.

The Nb/Ta ratio is also of significance as a tracer of magma sources. Increasing fractionation during magmatic evolution generally leads to increasing Ta content and decreasing Nb/Ta ratios (Liu 1987; Zhao et al. 2008), with silicic rocks therefore having the lowest ratios (Liu 1987). However, in alkaline magmas, the Nb/Ta ratio increases during evolution. Measured Nb/Ta ratios of the rhyolites are in the range of 17.65–17.99, similar to that of primitive mantle (Nb/Ta = 17.5) (Zhang et al. 2010) and Precambrian alkaline volcanic rocks of the North China Craton (Nb/Ta = 15.6 ± 2.9 to 18.8 ± 1.2) (Liu et al. 2005), and obviously higher than that of continental crust (Nb/Ta = 11) (Mclennan 1985).The rhyolite is therefore not a highly fractionated granite. Its source rocks have an affinity with original alkaline mantle-derived materials, and likely originated from crust composed of mafic mantle-derived rocks (alkaline basalt) and terrigenous clastic rocks rich in zircon (and hence Nb and Ta).

Ce and Eu anomalies

The positive Ce anomalies indicate high fO_2 and high Ce contents in the magma during petrogenesis. Igneous rocks generally have either no Ce anomaly or a weak negative one; ferromanganese nodules of colloidal origin have obvious positive anomalies, mid-ocean ridge around 400 km sediments have obvious negative anomalies (Ce/Ce* = 0.29), marine basin sediments have moderate negative anomalies (Ce/Ce* = 0.55), and continental margin clastic rocks have weakly negative or positive anomalies (0.90–1.30) (Murray et al. 1990; Zhao 1997). The Fe and Mn contents of the high Nb–Ta rhyolites are low, indicating no genetic connection between the positive Ce anomalies and marine ferromanganese nodules. Their petrogenesis is therefore not related to subduction of oceanic crust or deep-sea sediments.

The high valence and small ionic radius of Ce^{4+} result in its preferential adsorption by sediments, and Ce is therefore relatively enriched in terrigenous sediments while other (trivalent) REEs tend to remain in solution (Murray et al. 1990). Strongly positive Ce anomalies therefore imply that the source rock was a product of partial melting of terrigenous clastic rocks. They may also be related to the enrichment and melting of zircon in the source region. The zircon trace element diagram (Fig. 3) demonstrates that Ce and HREEs can be enriched in zircons, resulting in strongly positive Ce

anomalies. The positive Ce anomalies and high HREE contents of the rhyolites may therefore have been inherited from zircons, indicating that zircon-rich, terrigenous clastic rocks participated in source magma evolution.

The weathering of sedimentary clastic rocks in the source region would have resulted in negative Eu anomalies (Cullers et al. 1975) because Eu^{2+} is relatively soluble as compared with other REEs. Europium would be removed by chemical weathering in an open system, leaving Eu-poor sediments. Significant negative Eu anomalies may thus be caused by Eu depletion of the source rock and plagioclase in the source residue.

Major elements

Aluminous A-type granites are normally formed by the partial melting of lower crust rich in Al (Patino Douce 1997; Rajesh 2000). However, the high Nb–Ta rhyolites are weakly peraluminous, with Al-rich minerals in the source region, such as plagioclase and hornblende, having preferentially assimilated Al. The source rock of the rhyolites thus has an affinity with Al-rich ancient crust. In the mineral characterization diagrams ($Na_2O+K_2O+MgO+TiO_2$) vs (Na_2O+K_2O)/($FeO^T+MgO+TiO_2$) and ($Al_2O_3+FeO^T+MgO+TiO_2$) vs Al_2O_3/($FeO^T+MgO+TiO_2$) (Fig. 10a, b) (Patino Douce 1999), data for the samples plot in the metamorphic greywacke and basic argillaceous rock fields.

Sr–Nd isotopic compositions

The ($^{87}Sr/^{86}Sr$)i ratios of the rhyolites (0.70300–0.71160) vary greatly, and εSr(t) values (− 18.21 to + 102.94) are mostly positive. The ($^{143}Nd/^{144}Nd$)i ratios are in the range of 0.512537–0.512539, and εNd(t) values are positive (1.9–2.0). These factors indicate that the source was likely to have been a product of partial melting of ancient crust composed of pre-existing mantle-derived materials.

Physico-chemical conditions of rhyolite formation

The negative Eu anomalies and low Ca, Fe, Sr, and Mg contents of the rhyolites are consistent with melting of residual phases of hydrous tholeiite at temperatures of 650–800 °C and pressures of < 0.8 GPa. The residual phases are mainly Ca-rich plagioclase + amphibole ± orthopyroxene ± ilmenite (with no garnet) (Wu et al. 2002). Granite formed in this process is of the low-Sr/high-Yb type (Zhang et al. 2006). The rhyolite is thus a low-Sr/high-Yb-type granite, probably formed at very low pressures (< 0.5 GPa) at depths of < 30 km (Zhang et al. 2006). It is generally considered that A-type granite is low-fO_2 granite (Loiselle and Wones 1979; Martin 2006), although it may be generated under oxidizing conditions (Anderson and Morrison 2005; Dall'Agnol and Oliveira 2007). The positive Ce anomalies of the rhyolites indicate that they were formed in high-fO_2 conditions.

Magma source

The Kyihe high Nb–Ta rhyolite T_{2DM} age of 789–785 Ma suggests that the source rock was Neoproterozoic crustal basement, corresponding to Neoproterozoic Rodinia tectono-magmatic evolution (Zhou et al. 2016; Zeng et al. 2014) and the formation of khondalite in the Xingan Block (Zhou et al. 2011a; Zeng et al. 2014).

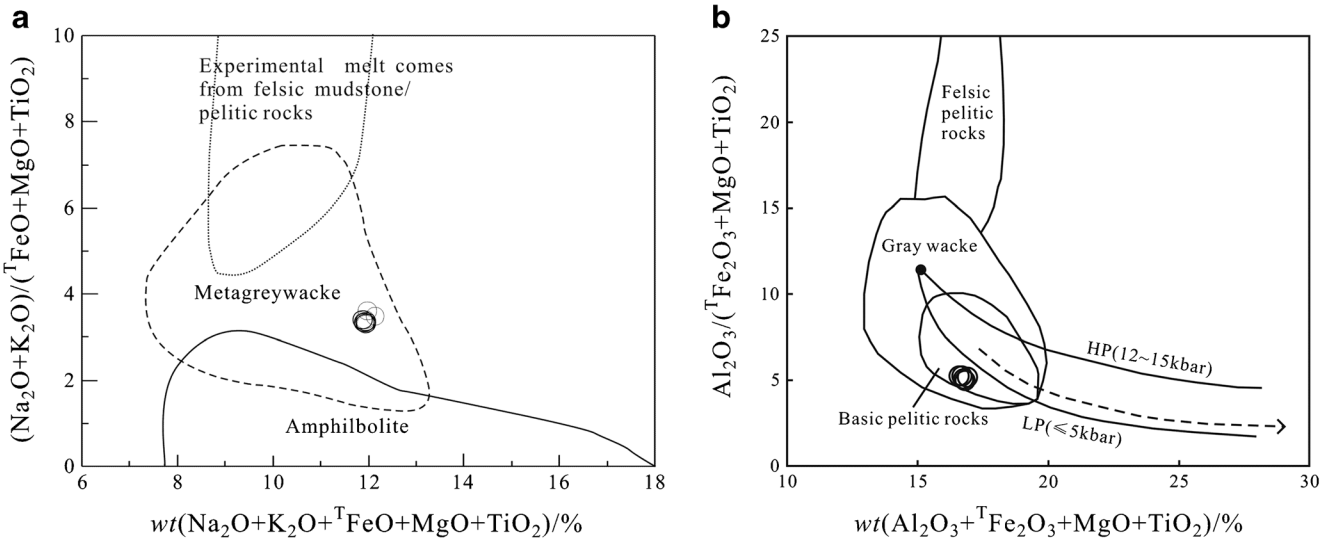

Fig. 10 $Na_2O+K_2O+FeO^T+MgO+TiO_2$–($Na_2O+K_2O$)/$FeO^T+MgO+TiO_2$(a) and $Al_2O_3+FeO^T+MgO+TiO_2$–Al_2O_3/$FeO^T+MgO+TiO_2$(b) diagrams of high Nb–Ta rhyolite (After Patino Dounce, 1999)

The metamorphic basement of the Xingan Block is represented by the Xinghua Ferry Group, which is widely exposed in the area between Xinghua–Central Xinlin–Jiagedaqi in the Huma area (northern Xingan Block) and the Zhalantun area (southern Xingan Block). Its main rock types include sillimanite–garnet-bearing gneiss, felsic gneiss, amphibolite, and graphite schist (HBGMRRGH 1993; Miao et al. 2007; Zhou et al. 2011a; Wu et al. 2012), and the protoliths of which can be divided into metamorphic plutonic rocks and metamorphic supracrustal rocks. The metamorphic supracrustal rock is a typical volcanic–sedimentary formation, including metamorphosed mafic volcanic and sedimentary rocks, such as metamorphosed clastic rocks (Biao et al. 1999; Sun et al. 2002; Liu 2007) with ages of 970–660 Ma (Luo et al. 1997; Wu et al. 2012; Miao et al. 2003; Zhou et al. 2011a, b). The rock complex comprises Al-rich schist–gneisses and amphibolites. The source rocks of the Al-rich schist–gneisses are mudstone and sandstone with negative Eu anomalies (Eu/Eu* = 0.32–0.79) and positive Ce anomalies (Ce/Ce* = 0.90–1.30), indicating an unstable continental margin sedimentary environment. The source rock of the amphibolites was weakly alkaline basalt (Zhou et al. 2016; Dong and Zhou 2012). The formation age and geochemical characteristics of metamorphic crustal rocks of the Xinghua Ferry Group, which form the basement of the Xingan Block, correspond to the characteristics of the source rocks of the rhyolites.

Petrogenesis

In the Upper Jurassic (155 Ma), the northern segment of the Daxingan Mountains was in an intraplate extensional tectonic setting in which the thinned crust was underplated by mantle-derived basaltic magma. This resulted in the partial melting of crustal rocks of the basement Xinghua Ferry Group as the pressure decreased and temperature increased. The volcanic–sedimentary formation of Xinghua Ferry Group supracrustal rocks included metamorphosed mafic volcanic and terrigenous clastic rocks. It is speculated that the latter was rich in zircon, and hence Nb and Ta. Zircon and garnet were melting phases under shallow, low-pressure (< 30 km and < 0.8 GPa), and high fO_2 conditions during the melting of supracrustal rocks in which the rhyolitic magma was formed, whereas a residual mineralogy of Ca-rich plagioclase, amphibole, and orthopyroxene remained in the source.

Conclusions

(1) Zircons in the high Nb–Ta rhyolite display magmatic oscillatory zoning and have the same REE compositions as crustal magmatic zircons. A U–Pb age of 156 ± 1 Ma indicates that the rhyolites formed during the Upper Jurassic.

(2) The rhyolites are characterized by high SiO_2 and alkali contents; low Fe, Ca, and Mg contents; and a weakly peraluminous nature, indicating that they are high-K calc-alkaline rocks. Their trace element contents indicate enrichment in Nb, Ta, Zr, Hf, Ce, and Rb and depletion in Sr, Eu, Ba, P, Ti, Co, and Ni. The rhyolites are thus low-Sr/high-Yb rhyolites.

(3) The T_{2DM} Nd model ages of the rhyolites range from 789 to 785 Ma, indicating a crustal growth event during the Neoproterozoic, with crustal material originating from the depleted mantle or partial melting of juvenile crust. The εSr(t) values of the rocks (− 18.21 to + 102.94) are variable and mostly positive, and εNd(t) values are positive (1.9–2.0), indicating that the source comprised a mixture of crustal and mantle-derived materials.

(4) The rhyolite source rocks were metamorphosed supracrustal rocks comprising metamorphosed mafic volcanic and terrigenous clastic rocks of the Xinghua Ferry Group, which forms the basement of the Xingan Block.

(5) The high Nb–Ta rhyolite was formed in a tectonic setting which developed after the closure of the Mongolia–Okhotsk Ocean, or during the northward subduction of oceanic lithosphere under the Siberian Plate. Basaltic magma underplating provided the heat necessary for partial melting of metamorphic supracrustal rocks of the Xinghua Ferry Group. During partial melting of the source rocks, zircon and garnet were involved in melting, and plagioclase + amphibole + pyroxene were residual phases, due to the shallow depth, high temperature, and high oxygen fugacity melting conditions.

References

Anderson JL, Morrison J (2005) Ilmenite, magnetite, and peraluminous Mesoproterozoic anorogenic granites of Laurentia and Baltica. Lithos 80(1–4):45–60

Ballard JR, Michael P, Camllell HI (2002) Relative oxidation states of magmas inferred from Ce(IV)/Ce(III) inzircon: application to porphyry copper deposits of northern Chile. Contrib Mineral Petrol 144:347–364

Bao YWLJ, Su MR, Tan Q et al (2011) Revision of Middle Jurassic Wanbao Formation about China-Mongolia Border in the west of Manzhouli, Inner Mongolia. Geol Resour 20(1):12–15

Biao SH, Li YC, He XH et al (1999) The geochemical characteristics of the Xinghuadukou Group in the Lulin Forestry Center, Tahe, Heilongjiang Province. Reg Geol China 18(1):28–32

Burnham AD, Berry AJ (2012) An experimental study of trace element partitioning between zircon and melt as a function of oxygen fugacity. Geochim Cosmochim Acta 95:196–212

Chen ZG, Zhang LC, Lu BZ et al (2010) Geochronology and geochemistry of the Taiping-chuan copper–molybdenum deposit in Inner Mongolia, and its geological significances. Acte Petrologica Sinica 26(5):1437–1449

Chen YF, Wang GH, Duan BX (2012) Characteristics and chronology of the late Jurassic volcanic rocks in the Huiyinaobao area of Dongwuzhu, Inner Mongolia. Geol China 39(6):1690–1699

Cogné M, Morvan CL, Sirac C (2010). Mammifère non-humain transgénique pour la région constante de la chaîne lourde des iga humaines et ses applications (monoclonaux humanisés à destinée muqueuse)

Cullers RL, Chaudhuri S, Arnold B et al (1975) Rare earth distributions in clay minerals and clay-sized fraction of the Lower Permian Havensville and Eskridge shales of Kansas and Oklahoma. Geochim Cosmochim Acta 39(12):1691–1703

Dall'Agnol R, Oliveira DCD (2007) Oxidized, magnetite-series, rapakivi-type granites of Carajás, Brazil: implications for classification and petrogenesis of A-type granites. Lithos 93(3–4):215–233

Dong C, Zhou JB (2012) Geochemistry of ~500Ma Pan-African khondalite series in west of NE China and tectonic implications. Acta Petrol Sin 28(9):2866–2878

Du Y, Liu ZH, Cui WL et al (2017) Formation age and geochemical characteristics of volcanic rocks from Manketouebo Formation in Keyihe area, Da Hinggan Mountains and its tectonic implications. Global Geol 36(1):54–65

Fan WM, Guo F, Wang YJ et al (2003) Late Mesozoic calcalkaline volcanic of post-orogenic extension in the northern Da Hinggan Mountains, northeastern China. J Volcanol Geotherm Res 121: 115–135

Ge WC, Lin Q, Sun DY et al (1999) Geo-chemical characteristics of the Mesozoic basalts in Da Hinggan Ling: evidence of the mantle-crust interaction. Acta Petrol Sin 15(3):397–407

Ge WC, Sui ZM, Wu FY et al (2007a) Zircon U-Pb ages, Hf isotopic characteristics and their implications of the Early Paleozoic granites in the northeastern Da Hinggan Mts., northeastern China. Acta Petrol Sin 23(2):423–440

Ge WC, Wu FY, Zhou CY, Zhang JH (2007b) Porphyry Cu-Mo deposits in the eastern Xing'an-Mongolian Orogenic Belt: mineralization ages and their geodynamic implications. Chin Sci Bull 52(24): 3416–3427

Gou J, Sun DY, Zhao ZH et al (2010) Zircon LA –ICPMS U –Pb dating and petrogenesis of rhyolites in Baiyingaolao Formation from the southern Manzhouli, Inner Mongolia. Acta Petrol Sin 26(1):333–344

Guo ZJ, Li JW, Huang GJ et al (2014) Sr-Nd-Pb-Hf isotopic characteristics of ore-bearing granites in the Honghuaerji scheelite deposit, Inner Mongolia. Geol China 41(4):1226–1241

Heilongjiang Bureau of Gology and Mineral Resources (1993) Regional Geology of Heilongjiang Province. Geological Publishing House, Beijing, pp 1–734

Hong DW, Wang SG, Xie XL et al (2000) Genesis of positive ε(Nd,t) granitoids in the Da Hinggan Mountains. Earth Sci Front 7(2):441–456

Hong DW, Wang SG, Xie XL et al (2003) Correlation between continental crustal growth and supercontinental cycle: evidence from the granites with positive εNd in the Central Asian Orogenic Belt. Acta Geol Sin 77(2):203–209

Hoskin PWO, Schaltegger U (2003) The composition of zircon and igneous and metamorphic petrogenesis. Rev Mineral Geochem 53(1): 27–55

Inner Mongolia Bureau of Geology and Mineral Resources (1991) Regional geology of Inner Mongolia. Geological Publishing House, Beijing, pp 1–725

Ji Z (2017) Petrogenesis and tectonic implications of volcanic rocks from the Manketouebo Formation in the Wuchagou region, central Great Xing'an Range. Jilin University, Jilin

Jiang SH, Nie FJ, Su YJ et al (2010) Geochronology and origin of the Erdenet superlarge Cu-Mo deposit in Mongolia. Acta Geosci Sin 31(3):289–306

Li GM, Li JX, Qin KZ, Zhang TP, Xiao B (2006) Preliminary study on alteration and mineralization features and high-oxidated ore-forming fluids at Duobuza super-large Au-rich porphyry Cu deposit, western Tibet. Mineral Deposits 25(supp):411–414 (in Chinese with English abstract)

Li PC, Li SC, Liu ZH et al (2016) Formation age and environment of the volcanic rocks from the Manketouebo Formation in Linxi area, Inner Mongolia. Global Geol 35(1):77–88

Lin Q, Ge WC, Sun DY et al (1998) Tectonic significance of Mesozoic volcanic rocks in northeastern China. Sci Geol Sin 2:129–139

Liu YJ (1987) Introduction to elemental geochemistry. Geological Publishing House, Bath

Liu XG (2007) The geological-geochemical characteristics and the structural significance of the Xinghuadukou Rock Group of Paleoproterzoic in Heihe area. Jilin University, Jilin

Liu JM, Zhang R, Zhang QZ (2004) The regional metallogeny of Da Hinggan Ling, China. Earth Sci Front 11(1):269–277

Liu YS, Gao S, Wang XC et al (2005) Nb/Ta variations of mafic volcanic on the Archean-Proterozoic boundary: implications for the Nb/Ta imbalance. Sci China(D) 48(8):1106–1119

Loiselle MC, Wones D (1979) Characteristics and origin of anoro-genic granites. Geological Society of America, Abstracts with Programs 11:468

Luo Y, Wang ZB, Zhou DA (1997) The geologic characteristics and prospecting prospect of Eerguna super large volcanic hydrothermal type uranium metallogenic belt. J East China Geol Inst 20(01):2–11

Martin RF (2006) A-type granites of crustal origin ultimately result fromopen-system fenitization-type reactions in an extensional environment. Lithos 91:125–136

Maruyama S, Isozaki Y, Kimura G et al (1997) Paleogeographic maps of the Japanese Islands: plate tectonic synthesis from 750 Ma to the present. Island Arc 6(1):121–142

Mass R, Kinny PD, Williams IS et al (1992) The Earth's oldest known crust: a geochronological and geochemical study of 2900-4200 Ma old detrital zircons from Mt. Narryer and Jack Hills, Western Australia. Geochim Cosmochim Acta 56:1281–1300

Mcdonough WF, Sun S (1995) The composition of the Earth. Chem Geol 120(3/4):223–253

Mclennan (1985) The continental crust: its composition and evolution. Geol Mag 6: 673–674

Meng QR (2003) What drove Late Mesozoic extension of the northen China Mongolia tract? Tectonophysics 369:155–174

Meng E, Xu WL, Yang DB et al (2011) Zircon U –Pb chronology, geochemistry of Mesozoic volcanic rocks from the Lingquan basin in Manzhouli area, and its tectonic implications. Acta Petrol Sin 27(4): 1209–1226

Metelkin DV, Vernikovsky VA, Kazansky AY et al (2010) Late Mesozoic tectonics of Central Asia based on paleomagnetic evidence. Gondwana Res 18(2):400–419

Miao LC, Fan WM, Zhang FQ et al (2003) Zircon SHRIMP geochronology of the Xingkailing-Kele complex in the northwestern Lesser Xing'an Range, and its geological implication. Chin Sci Bull 48(22):2315–2323

Miao LC, Liu DY, Zhang FQ et al (2007) Zircon SHRIMP U-Pb ages of the "Xinghuadukou Group" in Hanjiayuanzi and Xinlin areas and the "Zhalantun Group" in Inner Mongolia, Da Hinggans Mountains. Chin Sci Bull 52:112–1134

Mou BL (1999) Elemental geochemistry. The Peking University Publishing House, Beijing

Murray RW, Buchholtz TBMR, Jones DL et al (1990) Rare earth elements as indicators of different marine depositional environments in chert and shale. Geology 18(3):268–271

Natal'in BA, Borukayev CB (1991) Mesozoic sutures in the southern Far East of USSR. Geotectonics 25(1):64–74

Patino Douce AE (1997) Generation of metaluminous A-type granites by low-pressure melting of calc-alkaline granitoids. Geology 25(8): 743–746

Patino Douce AE (1999) What do experiments tell us about the relative contributions of crust and mantle to the origin of granitic magmas? Geol Soc Lond Spec Publ 168(1):55–75

Pei J, Sun Z, Jing L et al (2011) A paleomagnetic study from the Late Jurassic volcanics (155 Ma), North China: implications for the width of Mongol–Okhotsk Ocean. Tectonophysics 510(3–4):370–380

Qu GS (1997) Stratigraphy (lithostratic) of Heilongjiang Province. China University of Geosciences Press, Wuhan

Rajesh HM (2000) Characterization and origin of a compositionally zoned aluminous A-type granite from South India. Geol Mag 137(3):291–318

Reid JBJ, Murray DP, Hermes OD et al (1993) Fractional crystallization in granites of the Sierra Nevada: how important is it? Geology 21(7): 587

Şengör AMC, Natal'in B A, Burtman V S (1993) Evolution of the Altaid tectonic collage and Palaeozoic crustal growth in Eurasia. Nature 364(6435):299–307

Şengör AMC, Natal'in BA, Yin A, Harrison TM (1996) Paleotectonics of Asia: fragments of a synthesis. The tectonic evolution of Asia. Cambridge University Press, Cambridge, pp 486–640

Shao JA, Zhang LQ (1999) Magmatism in the Mesozoic extending orogenic process of Hinggan Mts. Earth Sci Front 6(4):339–346

Shao JA, Mou BL, He GQ et al (1997) The tectonic superposition process of the ancient Asian and Pacific domains in the north part of North China. China Science Press 27(5):390–394

Shao JA, Zhang LQ, Mou BL (1998) The Mesozoic tectonic thermal evolution of the middle and south sections of the Daxingan Mountains. China Science Press 28(3):193–200

Shi SS, Wang YL, Shi JM et al (2014) Structural characteristics of the southern margin of the middle Jurassic Mohe Basin: geological implication. Geol Resour 23(6):511–514

Sun S, Mcdonough WF, Saunders AD, Norry MJ (1989) Chemical and isotopic systematics of oceanic basalts: implications for mantle composition and processes. Magmatism in the ocean basins. Geol Soe Spec Publ 42:313–345

Sun GR, Li YC, Zhang Y (2002) The basement tectonics of Ergun massif. Geol Resour 03:129–139

Sun DY, Gou J, Ren YS et al (2011) Zircon U-Pb dating and study on geochemistry of volcanic rocks in Manitu Formation from southern Manchuria, Inner Mongolia. Acta Petrol Sin 27(10):3083–3094

Voo RVD, Spakman W, Bijwaard H (1999) Mesozoic subducted slabs under Siberia. Nature 397(6716):246–249

Wang F, Zhou XH, Zhang LC et al (2006) Late Mesozoic volcanism in the Great Xing'an Range (NE China): timing and implications for the dynamic setting of NE Asia Collected paper abstracts. Institute of Geology and Geophysics, Chinese Academy of Sciences 2007: 179–198

Wang J, Chen SW, Ding QH (2013a) Ziron U-Pb dating and geochemical characteristics of detrital rocks and their constraints on the provenance of Middle Jurassic Wanbao Formation in Tuquan basin. Geol Bull China 32(8):1224–1235

Wang JG, He ZH, Xu WL (2013b) Petrogenesis of riebeckite rhyolites in the southern Da Hinggan Mts: geohronological and geochemical evidence. Acta Petrol Sin 29(3):853–863

Wang CY, Wang DB, Qu JJ (2017) Chronology and geochemistry of rhyolites in Manketou'ebo Formation from Keyihe area, north-central Greater Xing'an Range. J Heilongjiang Univ Sci Technol 27(1):46–50

Whalen JB, Currie KL, Chappell BW (1987) A-type granites: geochemical characteristics, discrimination and petrogenesis. Contrib Mineral Petrol 95(4):407–419

Wu H (1996) Geology and mineral bureau of inner mongolia. Lithostratigraphy of Inner Mongolia, China University of Geosciences Press 256–264

Wu FY, Sun DY, Li HM, Jahn BM, Wilde S (2002) A-type granites in northeastern China: age and goechemical constraints on their petrogenesis. Chem Geol 187:143–173

Wu FY, Li XH, Yang JH et al (2007) Discussions on the petrogenesis of granites. Acta Petrol Sin 23(6):1217–1238

Wu FY, Sun DY, Ge WC, Zhang YB, Grant ML, Wilde SA, Jahn BM (2011) Geochronology of the Phanerozoic granitoids in northeastern China. J Asian Earth Sci 41(1):1–30

Wu G, Chen Y, Chen Y, Zeng Q (2012) Zircon U–Pb ages of the metamorphic supracrustal rocks of the Xinghuadukou Group and granitic complexes in the Argun massif of the northern Great Hinggan Range, NE China, and their tectonic implications. J Asian Earth Sci 49(3):214–233

Xu WL, Ji WQ, Pei FP, Meng E, Yu Y, Yang DB, Zhang X (2009) Triassic volcanism in eastern Heilongjiang and Jilin provinces, NE China: chronology, geochemistry, and tectonic implications. J Asian Earth Sci 34(3):392–402

Xu MJ, Xu WL, Meng E et al (2011) LA-ICP-MS zircon U-Pb chronology and geochemistry of Mesozoic volcanic rocks from the Shanghulin-Xiangyang basin in Ergun area, northeastern Inner Mongolia. Geol Bull China 30(9):1321–1338

Xu WL, Wang F, Pei FP et al (2013) Mesozoic tectonic regimes and regional ore-forming background in NE China: constraints from spatial and temporal variations of Mesozoic volcanic rock associations. Acta Petrol Sin 29(2):339–353

Yang Y, Gao FH, Chen JS et al (2012) Zircon U-Pb ages of Mesozoic volcanic rocks in Chifeng area. J Jilin Univ (Earth Sci Ed) s2:257–268

Zeng WS, Zhou JB, Dong C et al (2014) Subduction record of Mong-Okhotsk Ocean: constraints from Badaguan metamorphic complexes in the Erguma massif, NE China. Acta Petrol Sin 30(7): 1948–1960

Zhang JH (2009) Geochronology and geochemistry of the Mesozoic volcanic rocks in the Great Xing'an Range, northeastern China. China University of Geosciences, Beijing

Zhang Q, Wang Y, Li CD et al (2006) The Sr-Yb classification of granite and its geological significance. Acta Petrologica Scina 22(09): 2249–2269

Zhang Q, Pan GQ, Li CD et al (2007) Are discrimination diagrams always indicative of correct tectonic settings of granites? Some crucial questions on granite study (3). Acta Petrol Sin 23(11):2683–2698

Zhang JH, Ge WC, Wu FY, Wilde SA, Yang JH, Liu XM (2008) Large-scale Early Cretaceous volcanic events in the northern Great Xing'an Range, northeastern China. Lithos 102(1–2):138–157

Zhang JH, Gao S, Ge WC, Wu FY, Yang JH, Wilde SA, Li M (2010) Geochronology of the Mesozoic volcanic rocks in the Great Xing'an Range, northeastern China: implications for subductiion-induced delamination. Chem Geol 276:144–165

Zhang Q, Ran H, Li CD (2012) A-type granite: what is the essence? Acta Petrol Mineral 31(4):621–626

Zhang C, Yang WH, He ZH et al (2014) Chronology and geochemistry of rhyolites in Manketou'ebo Formation from Ta'erqi area, southern-center Greater Xing'an Range. Global Geol 33(2):255–265

Zhang YJ, Wu XW, Zhang C et al (2017) New evidences for dating of the Middle Jurassic Wanbao Formation in Longjiang Basin, western margin of Heilongjiang Province. Earth Sci Front 24(5):1–13

Zhao ZH (1997) The principle of trace element geochemistry. Science Press, p 128

Zhao B(2010a) Research on tectonic evolusion feature and origin mechanism in Hailar Basin. Dissertation, Daqing Pretroleum Insttitute

Zhao ZH (2010b) Trace element geochemistry of accessory minerals and its applications in petrogenesis and metallogenesis. Earth Sci Front 17(1):267–285

Zhao Y, Yang ZN, Ma XH (1994) Geoteconic transition from paleoAsian system and paleoTethyan system to paleo-pacific active continental margin in eastern Asia. Sci Geol Sin 2:105–119

Zhao ZH, Xiong XL, Wang Q et al (2008) Some aspects on geochemistry of Nb and Ta. Geochemica 37(4):304–320

Zhao LG, Yang XP, Zhao XM et al (2014) LA-ICP-MS U-Pb geochronology of the sedimentary rock and volcano rock zircons from the Emoerhe Group in the Mohe Basin and its geological significance. J Geomech 20(3):285–291

Zhou ZC, Jiang ZQ (2017) Geochemical characteristics and its genesis of volcanic rocks in the Manketouebo Formation in the Zaina banner, Inner Mongolia. West Resour 3:1–4

Zhou XH, Ying JF, Zhang LC (2009) The petrogenesis of Late Mesozoic volcanic rock and the contributions from ancient micro-continents: constraints from the zircon U-Pb dating and Sr-Nd-Pb-Hf isotopic systematics. Earth Sci 34(1):1–10

Zhou JB, Wilde SA, Zhang XZ, Zhao GC, Liu FL, Qiao DW, Ren SM, Liu JH (2011a) A > 1300km Late Pan-African metamorphic belt in NE China: new evidence from the Xing'an block and its tectonic implications. Tectonophysics 509(3–4):280–292

Zhou JB, Wilde SA, Zhang XZ, Ren SM, Zheng CQ (2011b) Early Paleozoic metamorphic rocks of the Erguna block in the Great Xing'an Range, NE China: evidence for the timing of magmatic and metamorphic events and their tectonic implications. Tectonophysics 499(1–4):105–117

Zhou JB, Zeng WS, Cao JL et al (2012) The tectonic framework and evolution of the NE China: from ~500Ma to ~ 180 Ma. J Jilin Univ (Earth Sci Ed) 42(5):1298–1329

Zhou JB, Shi AG, Jing Y (2016) The combined NE China blocks: tectonic evolution and supercontinent reconstrutions. J Jilin Univ (Earth Sci Ed) 46(4):1042–1055

Zindler A, Hart SR (1986) Chemical geodynamics. Annu Rev Earth Planet Sci 14:493–571

Zorin YA (1999) Geodynamics of the western part of the Mongolia–Okhotsk collisional belt, trans-Baikal region (Russia) and Mongolia. Tectonophysics 306(1):33–56